Effect of Solvent Quality and Electrostatic Interactions on Size and Structure of Dendrimers. Brownian Dynamics Simulation and Mean-Field Theory

Sergey V. Lyulin,[†] L. J. Evers,[‡] Paul van der Schoot,[‡] Anatolij A. Darinskii,[†] Alexey V. Lyulin,*[,‡] and M. A. J. Michels[‡]

Institute of Macromolecular Compounds, Russian Academy of Sciences, Bolshoj Prospect 31, St. Petersburg, 199004, Russia, and Group Polymer Physics, Eindhoven Polymer Laboratories and Dutch Polymer Institute, Technische Universiteit Eindhoven, P.O. Box 513, 5600 MB Eindhoven, The Netherlands

Received September 1, 2003; Revised Manuscript Received February 4, 2004

ABSTRACT: Conformational properties of neutral and charged dendrimers in dilute solutions of different quality have been investigated by a mean-field analytical approach and by Brownian dynamics (BD) computer simulation for systems up to generation six. Radial monomer distribution and mass distribution functions, radii of gyration, and structure factors have been studied as functions of solvent quality, effective charge of the terminal groups, and Debye screening radius. For high-generation dendrimers BD simulations show that the dendrimers hardly fluctuate. Swelling of both neutral and charged dendrimers is reasonably described by a generalized Flory mean-field theory in which the two-body virial term is replaced by the sum of the excluded-volume and two-body attraction terms. A non-Gaussian term taking into account the finite extensibility of spacers and a Coulomb term in the form of the Debye−Hückel approximation have been included as well. The θ-point for a single dendrimer molecule is defined as the characteristic energy of the excluded-volume interactions when the linear expansion factor α is equal to unity. In contrast to linear polymers, the θ-point defined in such way is different from that calculated as the characteristic energy when scaling relation for a good-solvent conditions stops to be valid. Dendritic terminal groups are distributed through the whole volume of the molecule, but the maximum of this distribution is shifted toward the periphery with increase of Debye screening radius and effective charge of a terminal group. It is shown that fractal dimension of a neutral dendrimer depends on both its generation number and spacer length.

1. Introduction

Dendrimers represent monodisperse macromolecules with regular and strongly branched architecture. In the late 1970s Buhleier et al.[1] carried out the first "cascade" synthesis of these macromolecules. The dendritic structures of polyamidoamine and arborol polymers have been studied later by Tomalia et al.[2,3] The unique architecture and monodisperse structure of dendrimers result in numerous previously unknown or significantly improved physical and chemical properties when compared to traditional linear polymers. Dendrimers have two major chemical environments: the surface chemistry due to the functional groups on the terminal generation, which is the surface of the dendritic sphere, and the sphere's interior, which is largely shielded from exterior environments due to the compact spherical shape. The existence of two different chemical environments in such a molecule implies many possibilities for dendrimer applications. They, for example, can be used as molecular cages for the direct transport of different compounds[4] such as drugs and DNA. Much of the interest in dendrimers involves their use as catalytic agents, in view of their high surface functionality and ease of recovery.

During the past two decades the efforts to understand the solution and bulk behavior of dendrimers have been intensified from both the theoretical and experimental sides. There is a rather large amount of theoretical and computer simulation studies where conformations and density profiles of dendrimers in solutions are considered. The theoretical consideration of neutral dendrimers began with the classical paper of de Gennes and Hervet,[5] based on a mean-field description of the starburst molecule in the limit of long flexible spacers between the trifunctional monomers. From the assumption that the monomers of each generation lie in a concentric shell, they concluded that the mean radial density of monomers in dendrimers increases with the distance from the dendritic core. This conclusion disagrees with the results of the modern computer simulations and scattering experiments.[6−8,34] In fact, the observed back-folding of dendrimer branches may lead to a decrease of the monomer density from the core to the periphery of a molecule. As shown in refs 6−8, the terminal groups are not fixed on the surface of a dendrimer, as predicted by de Gennes and Hervet, but rather distributed through the whole volume of the molecule. Such a behavior was explained by Boris and Rubinstein[9] and Ganazzoli et al.[10] on the basis of the Flory approach.[11] In particular, the swelling of a dendrimer in a good solvent below the starburst limit was successfully predicted. One caveat of this approach is that the intramolecular excluded-volume interactions were taken into account in the form of two-body interac-

[†] Russian Academy of Sciences.
[‡] Technische Universiteit Eindhoven.
* To whom correspondence should be addressed. E-mail a.v.lyulin@tue.nl.

10.1021/ma035286h CCC: $27.50
Published on Web 03/19/2004

tions only. This approximation breaks down for dendrimers of high generations and for poor-solvent conditions where attraction between monomers becomes significant.

The effect of the solvent quality on the dendrimer structure has been studied through molecular dynamics (MD) simulation by Murat and Grest.[6] Qualitative conclusions about the densifying of a dendrimer with increase of attraction between monomers were obtained. A more quantitative approach was suggested recently by Sheng et al.[12] They have performed off-lattice Monte Carlo (MC) simulations for dendrimers up to generation $g = 7$, with spacer length s varied between 1 and 50 units. The nonbonded monomers interacted via a square-well potential, and the quality of the solvent was varied by changing the depth of the well. Sheng et al. generalized the Boris and Rubinstein theory[9] by including both two- and three-body terms into the segment−segment interaction energy. For the N dependence of the gyration radius the scaling laws $R_g \sim N^{1/5}((g+1)s)^{2/5}$ and $R_g \sim N^{1/3}$ were predicted for good- and poor-solvent regimes, respectively. Good agreement between the MC simulation results and the predicted scaling relations has been shown.

Up to now the majority of the analytical and simulation studies is devoted to the investigation of the properties of neutral dendrimers. However, the most widespread are water-soluble dendrimers containing functional groups that can be charged by the change of the pH of the solution. As examples, the poly(propyleneimine) Astramol and poly(amidoamine) dendrimers can be mentioned.[7,8,13−15] Such dendrimers show polyelectrolyte behavior, and charge−charge repulsions force the charged moieties as far apart as possible. At the same time the hydrophobic attraction between functional groups leads to the compaction of the individual dendrimers.

To our knowledge there exist only two papers devoted to the computer simulation of charged dendrimers. Recently, Welch and Muthukumar[7,8] carried out an MC simulation study of the statistical properties of charged dendrimers in dilute solution. Dendrimers with charges in all branching points, with charged terminal groups only, have been simulated. It was shown that the charged dendrimers should undergo significant change of their size and density profile by the change of the solution salt concentration. For example, the terminal groups are significantly shifted to the exterior by a decrease of the salt concentration. However, the simulation results were not compared with theoretical predictions.

The key purpose of the present paper is to investigate the structure of a dendritic molecule under the influence of different kinds of interactions: excluded volume, solvent quality, and Coulombic interactions. Two different approaches have been implemented—mean-field theory and Brownian dynamics simulation. In the first approach a generalization of the Flory mean-field theory for the case of a charged dendrimer has been developed. The two-body virial term used by Boris and Rubinstein[9] is replaced now by the sum of the excluded-volume and two-body attraction terms. A non-Gaussian term taking into account the finite extensibility of spacers (which is important for the short spacers consisting of rigid elements) has been included into the elastic energy as well. Finally, the Coulombic term has been added in the Debye−Hückel form. We also perform Brownian dynamics (BD) simulations of neutral dendrimers in solvents of different quality and simulations of charged dendrimers with varying strengths of the electrostatic interactions. In both approaches we focus on properties related to total size, internal mass distribution, position of the terminal groups, and overall structure.

The remainder of the paper is organized as follows. In section 2 the dendrimer model and simulation method are introduced. In section 3 the mean-field theory for neutral and charged dendrimers is presented. Swelling and collapse of the neutral dendrimers in solvents of different quality is described. The θ-point for a single dendrimer molecule is defined as the characteristic energy of the excluded-volume interactions when the linear expansion factor α is equal to unity. This definition is compared to that of Sheng et al.[12] The influence of the electrostatic interactions and stretching of the dendritic branches beyond the Gaussian approximation is considered as well. In section 4 the results of the BD simulations for the mean-squared radii of gyration and fractal dimensions of dendrimers are discussed and compared with theoretical predictions. Moreover, the radial distribution of monomers, the structure factor, and the asphericity parameter have been simulated. Conclusions are summarized in section 5.

2. Dendrimer Model and Simulation Algorithm

2.1. Dendrimer Model. The model and numerical algorithm of BD is identical to that used previously for the study of neutral dendrimers by Lyulin et al.[16−19] We consider the bead−rod freely jointed toy model of a dendrimer (Figure 1a). The dendrimer is represented as a system of beads connected by the rigid bonds of length l. No valence-angle and torsional potentials are taken into consideration. Dendrimers with three functional groups and a three-functional core are studied. Dendrimer generations g start from the generation $g = 0$. This first dendrimer consists of four beads including the core. The total number N of beads in a dendrimer with g generations is defined as

$$N = 3s(2^{g+1} - 1) + 1 \tag{1}$$

where s is the number of bonds between the branching points. In computer simulations we consider two cases, $s = 1$ and $s = 2$.

All nonbonded beads interact via a Lennard-Jones potential in which the attractive term is modified by a dimensionless screening factor β_{LJ}

$$U_{LJ}(r_{ij}) = 4\epsilon_{LJ}\left[\left(\frac{\sigma}{r_{ij}}\right)^{12} - \beta_{LJ}\left(\frac{\sigma}{r_{ij}}\right)^{6}\right] \tag{2}$$

where r_{ij} is the distance between ith and jth beads and ϵ_{LJ} and σ are the energy and length parameters. Note that this choice corresponds to the parameters $\epsilon = \epsilon_{LJ}\beta_{LJ}^2$ and $\sigma' = \sigma(\beta_{LJ})^{-1/6}$ for the standard Lennard-Jones potential. The quality of the solvent is regulated by changing the value of β_{LJ}. Case $\beta_{LJ} = 0$ corresponds to the athermal solvent. The values $\sigma = 0.8l$ and $\epsilon_{LJ} = 0.3k_bT$ are used as proposed by de la Torre et al.[20] to correctly reproduce the molecular weight dependence of the mean-squared end-to-end distance of a linear chain in a Θ-solvent. The shifted Lennard-Jones potential

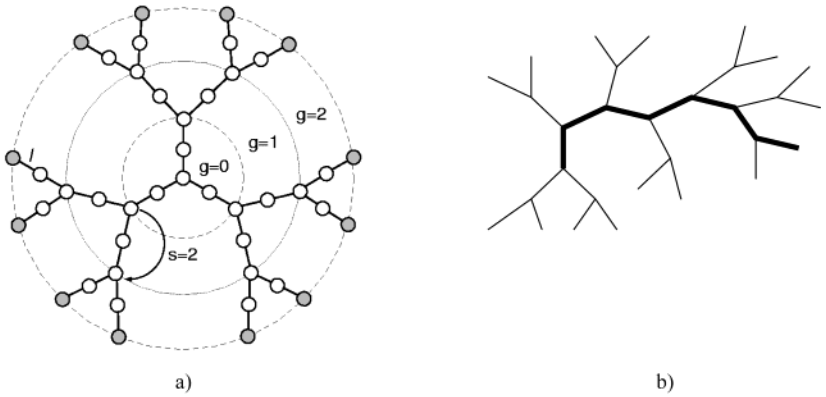

Figure 1. (a) Freely jointed bead−rod model employed in this study: the above example can be characterized as a dendrimer with $g = 2$ and $s = 2$. (b) A single linear branch (consisting of 7 monomers) in a $g = 6$ dendrimer. With the numeration of generation starting from zero, the contour length of the path is equal to $(g + 1)s$.

$$\tilde{U}_{\mathrm{LJ}}(r) = U_{\mathrm{LJ}}(r) - 4\epsilon_{\mathrm{LJ}}\left(\left(\frac{\sigma}{r_{\mathrm{cut}}}\right)^{12} - \beta_{\mathrm{LJ}}\left(\frac{\sigma}{r_{\mathrm{cut}}}\right)^{6}\right) \quad (3)$$

with $r_{\mathrm{cut}} = 2.5\sigma$ is used in the present simulation.

For charged dendrimers we only consider the case where terminal beads are charged, all with the same charge *ze*. Such a situation is realized, for example, for PAMAM and other dendrimers in water solutions at neutral pH.[21] Similar to Welch and Muthukumar,[7,8] we suppose that the *j*th charged bead interact with all other beads via the Debye−Hückel potential (electrostatic screened Coulomb potential)

$$\frac{U_j^{\mathrm{C}}}{k_{\mathrm{b}}T} = \lambda_{\mathrm{B}}\sum_{i=1}^{N_T}\frac{z^2\exp(-kr_{ij})}{r_{ij}} \quad (4)$$

where r_{ij} is the distance between terminal beads i and j, λ_{B} is the Bjerrum length describing the strength of the Coulomb interaction in a medium with dielectric constant $\tilde{\epsilon}$

$$\lambda_{\mathrm{B}} = \frac{e^2}{4\pi\tilde{\epsilon}k_{\mathrm{b}}T} \quad (5)$$

and k is the inverse Debye length, which describes the screening of the electrostatic interactions due to the presence of counterions and salt in the solution

$$k^2 = 4\pi\lambda_{\mathrm{B}}\sum_i z_i{}^2 c_i \quad (6)$$

Here c_i is the concentration of ith ion and z_i is its valence. The value of λ_{B} in water at room temperature is about 7 Å and is close to the segment length for a usual flexible polymer. Therefore, we could put $\lambda_{\mathrm{B}} = l$ without much practical loss of generality.

2.2. Simulation Algorithm. In this paper we consider a dilute solution of dendrimers without hydrodynamic interactions (HI). The neglect of HI accelerates the calculations and does not influence the equilibrium properties. All beads of a dendrimer are characterized by the friction coefficient ζ. The finite-difference numerical scheme implemented here is based on the Ermak−McCammon equation[22,23]

$$\vec{r}_i = \vec{r}_i^{\,0} + \frac{\Delta t}{k_{\mathrm{b}}T}\sum_j D_{ij}^0\cdot\vec{F}_j^0 + \vec{\Phi}_i^0(\Delta t), \quad i = 0, ..., N \quad (7)$$

where $\vec{r}_i^{\,0}$ is the position vector for ith bead before a time step Δt, the core of the molecule is defined by $i = 0$, and D_{ij}^0 is the translational diffusion tensor. The solvent is represented by a structureless continuum that generates a random noise $\vec{\Phi}_i^0$, which has a zero mean and a variance−covariance matrix given by

$$\langle\vec{\Phi}_i^0(\Delta t)\cdot\vec{\Phi}_j^0(\Delta t)\rangle = 2\Delta t D_{ij}^0 \quad (8)$$

In the absence of hydrodynamic interactions the diffusion tensor D_{ij}^0 is diagonal

$$D_{ii}^{(\alpha\beta)0} = (k_{\mathrm{b}}T/\zeta)\delta_{\alpha\beta}, \quad i = 0, ..., N \quad (9a)$$

$$D_{ij}^{(\alpha\beta)0} = 0, \quad i \neq j = 0, ..., N \quad (9b)$$

where α and β represent the x, y, or z components of a Cartesian coordinate system and $\delta_{\alpha\beta}$ is the Kronecker symbol. The force $\vec{F}_j^0$ acting on a bead j is given by

$$\vec{F}_j^0 = -\sum_{k=1}^{N}\mu_k\left(\frac{\partial\nu_k}{\partial\vec{r}_j}\right)_{r^0} - \partial\tilde{U}_{\mathrm{LJ}}/\partial\vec{r}_j^{\,0} - \partial U_j^{\mathrm{C}}/\partial\vec{r}_j^{\,0} \quad (10)$$

where ν_k is the equation for the kth rigid constraint, $\nu_k = (1/2)(\vec{r}_{k+1} - \vec{r}_k)^2$, and μ_k is the corresponding Lagrange multiplier.

The SHAKE algorithm[24,25] with relative tolerance of 2×10^{-6} is used to maintain a fixed bond length. In the simulation dimensionless quantities are used in which the bond length l, the thermal energy $k_{\mathrm{b}}T$, and the translational friction coefficient $\zeta = 6\pi\eta_0 a$ (a is the hydrodynamic radius of a bead) are all set to unity. It follows that time is in units $\zeta l^2/k_{\mathrm{b}}T$, the diffusion coefficient in units $k_{\mathrm{b}}T/6\pi\eta_0 a$, and the force in units $k_{\mathrm{b}}T/l$. The dimensionless integration step is equal to $\Delta t = 10^{-4}$. This value of Δt was chosen in order to have as the maximum displacement of a bead less than 10% of the bond length.

2.3. Generating the Initial Configuration. The initial configuration of a dendrimer is built using a procedure similar to that proposed by Murat and Grest.[6] The core bead is put in the center of the reference frame and is taken to be a small sphere of radius 0.5σ. Onto the core bead, along the X, Y, and Z axes, three chains of s monomers each are attached, which constitute the generation $g = 0$ dendrimer. The next generation is built adding two chains to each of the free ends of the $g = 0$

dendrimer. The distance between a newly added bead and all the previous beads is constrained to be larger than some distance $r_{min} = 0.8\sigma$. Obviously, as g increases, it becomes increasingly difficult to fulfill the constraint of no overlap. If a bead cannot be inserted after a set of 1000 trials, the whole dendrimer is discarded, and the whole process is started again with a new random-number seed. This procedure allows the construction of the initial configuration of dendrimers up to $g = 6$.

2.4. Simulation Details. Each initial configuration is equilibrated for 5×10^5 time steps. The number of simulation steps in each production run is increased until the difference between the calculated mean values of the diagonal elements of the gyration tensor is less than 5%. Production runs of about 4×10^6 time steps have been used for all generation numbers. During each production run the normalized autocorrelation function of the squared radius of gyration is calculated according to

$$C_{R_g^2}(t) = \frac{\langle R_g^2(0)\, R_g^2(t)\rangle - \langle R_g^2\rangle^2}{\langle R_g^4\rangle - \langle R_g^2\rangle^2} \tag{11}$$

The correlation time, $\tau_{R_g^2}$, is defined as the value where $C_{R_g^2}(\tau_{R_g^2}) = 1/e$. This correlation time increases with increasing generation number and decreases with increasing Bjerrum length or Debye screening radius. The total length of each production run was larger than $100\tau_{R_g^2}$.

3. Mean-Field Approximation for Neutral and Charged Dendrimers

3.1. Mean-Field Approximation. A single linear polymer chain in a good solvent fluctuates strongly. Flory[11] introduced a mean-field approximation which neglects these fluctuations but, surprisingly, predicts various polymer characteristics very accurately. For the problem in hand, the method implies that the excluded-volume interactions can be described in terms of uncorrelated collisions in a cloud of disconnected particles and that the most probable macroscopic state may be found by minimizing a Helmholtz free energy. The topology of a dendrimer suggests that the fluctuations are much smaller than in a single linear chain because dendrimers are much denser. Therefore, the mean-field approximation should reasonably accurately predict the equilibrium characteristics of dendrimers.

3.1.1. Swelling and Collapse of Neutral Dendrimers. Boris and Rubinstein[9] considered a mean-field Flory-type theory for expansion of a single dendrimer taking into account two-body excluded-volume interactions only. They suggested that the size of a dendrimer is proportional to the size of a single linear branch (Figure 1b). A scaling Ansatz for the free energy of a single linear branch of monomers in a generation-g dendrimer (remember that generations are numbered from zero) was written as[9]

$$\frac{F_F}{k_bT} \approx \frac{F_{el}}{k_bT} + \frac{\Delta F_{conf}}{k_bT} + (g+1)s\phi = \frac{3}{2}\alpha^2 - 3\ln\alpha + (g+1)s\phi_0\alpha^{-3} \tag{12}$$

where $F_{el}/k_bT = {}^3/_2\alpha^2$, $\Delta F_{conf}/k_bT = -3\ln\alpha$, $\alpha \equiv R_g/R_{g0}$ is the linear expansion factor, R_{g0} is the radius of gyration of an ideal Gaussian dendrimer, and R_g is its actual radius of gyration. The mean segment density, ϕ, is written as

$$\phi = \frac{N\nu}{R_g^3} = \frac{N\nu}{R_{g0}^3}\alpha^{-3} \equiv \phi_0\alpha^{-3} \tag{13}$$

where N is the total number of monomers in the whole dendrimer, ν is the excluded-volume parameter, and ϕ_0 is the effective internal density of ideal dendrimers. The first term in eq 12 gives the entropic contribution to the free energy due to stretching of the branch advanced by Flory.[26] The second term is the confinement entropy. The third term represents the free energy due to the excluded-volume interactions of the linear path of monomers with the monomers of the rest of a dendrimer.

To include three- and higher-body excluded-volume interactions, the third term in eq 12 for the free energy needs to be generalized. We replace it by the sum of repulsion and attraction terms. Using a free-volume type of approach, we can describe the excluded-volume repulsion as

$$-(g+1)s\ln\left(1 - \frac{\phi}{\phi_{max}}\right) \tag{14}$$

where ϕ_{max} is the maximum attainable density, which is the density of the generation-g_{max} dendrimer (starburst), beyond which the dendrimer cannot grow due to overcrowding. Expansion of this expression in a series of ϕ gives a standard virial expansion for systems with purely repulsive interactions described by the excluded-volume parameter ν. The beads may also interact via a van der Waals attraction, which is described here by an additional term in the free energy, $(g+1)s\phi\epsilon$, where $\epsilon > 0$ is the strength of the van der Waals attraction between the beads. Within this admittedly crude approximation we can combine the van der Waals repulsion and attraction and rewrite eq 12 as

$$\frac{F_{F+VdW}}{k_bT} = \frac{F_{el}}{k_bT} + \frac{\Delta F_{conf}}{k_bT} + \frac{\Delta F_{VdW}}{k_bT} \tag{15a}$$

$$\frac{\Delta F_{VdW}}{k_bT} = -(g+1)s\ln\left(1 - \frac{\phi}{\phi_{max}}\right) - (g+1)s\phi\epsilon \tag{15b}$$

As pointed out by Birshtein and Pryamitsyn[27] for the case of a poor solvent, $\alpha < 1$, the first two terms in eq 15 should be rewritten as $F_{el}/k_bT + \Delta F_{conf}/k_bT \approx {}^9/_4\alpha^{-2} + {}^9/_2\ln\alpha$. This change introduces only minor corrections to the calculations because the contribution from the excluded-volume and attraction terms is dominant. Note that the free energy, eq 15, holds only for dendrimers that are not overstretched because the entropic terms hold only in the Gaussian approximation.

The equilibrium size of the dendrimer in terms of the linear-expansion factor, α, is found by minimizing the free energy, giving

$$\alpha^5 - \alpha^3 - (g+1)s\frac{\phi_0}{\phi_{max} - \phi_0\alpha^{-3}} + (g+1)s\phi_0\epsilon = 0 \tag{16}$$

Without loss of generality the maximum density can be taken as $\phi_{max} = 1$ because ϕ_{max} scales with ϵ: suppose $\phi'_{max} = \gamma\phi_{max}$ and $\phi'_0 = \gamma\phi_0$, then $\epsilon' = \epsilon/\gamma$. The numerical

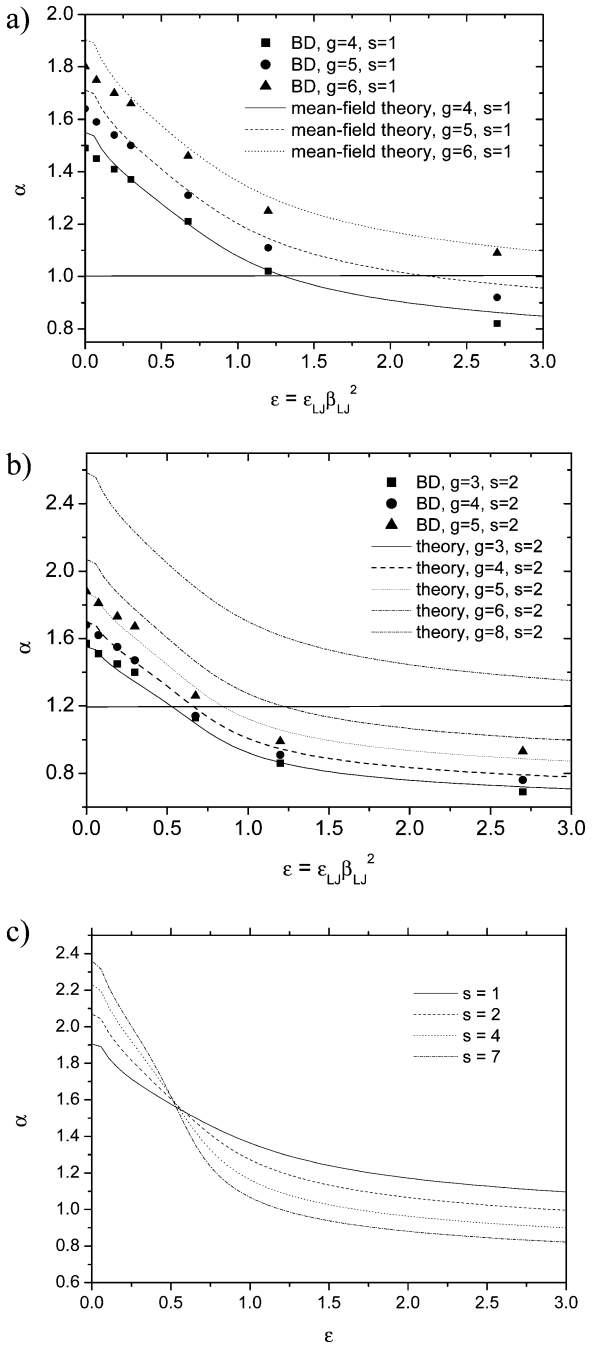

Figure 2. (a) Linear-expansion factor $\alpha = R_g/R_{g0}$ as a function of the solvent quality obtained from the simulation (BD) and the mean-field theory, eq 27. The results are shown for neutral dendrimers with spacer lengths $s = 1$. For higher generation numbers (theoretical curves) a collapse seems impossible because the van der Waals energy has to be unphysically increased. (b) The same results for $s = 2$. (c) The same theoretical results for a $g = 6$ neutral dendrimer with spacer lengths $s = 1$, 2, 4, and 7. The dendrimers can collapse more easily with increasing spacer length.

solution of eq 16 for dendrimers of generation $g = 3-8$ and spacer length $s = 1$, 2 is shown in Figure 2a,b. It shows a strong swelling behavior ($\alpha > 1$) of dendrimers for $\epsilon \rightarrow 0$ and a collapse ($\alpha < 1$) for not too high generation numbers, although not as pronounced as in the case of a single linear chain. The latter is due to the fact that a linear chain is a much more rarified object. With increasing generation this collapse seems to become impossible. In Figure 2c the numerical solutions of eq 16 for dendrimers of generation $g = 6$ and spacer length $s = 1$, 2, 4, and 7 are shown. The increase of the spacer length makes the dendrimer more rarified, which results in an easier (at smaller values of ϵ) collapse of a dendrimer with increasing the spacer length.

It is possible to obtain the scaling relations for the molecular-weight dependence of R_g^2 for two limiting cases, corresponding to the athermal and poor-solvent regimes. In the first regime $\alpha \gg 1$ and $\epsilon = 0$, and eq 16 is simplified as

$$\alpha^5 - (g+1)s\frac{\phi_0}{\phi_{max}} = 0 \tag{17}$$

For an ideal Gaussian branch we have $R_{g0}^2 \sim (g+1)s$, which gives

$$R_g^2 \sim \nu^{2/5}(s(g+1))^{4/5}N^{2/5} \tag{18}$$

Neglecting the logarithmic correction $s(g+1) \sim \ln N$, we obtain $R_g \sim N^{1/5}$ in accordance with the self-consistent-field results of de Gennes and Hervet.[5] For poor-solvent conditions (large ϵ and small α) eq 16 gives

$$R_g^2 \sim ((g+1)s\nu\epsilon)^{2/3}N^{2/3} \tag{19}$$

Apart from a logarithmic correction, this gives a compact structure, $R_g \sim N^{1/3}$. Similar scaling laws for these two limiting cases have been obtained by Sheng et al.[12]

An interesting topological aspect of dendrimers is the concept of limited growth, i.e., the impossibility to grow beyond the starburst limit.[5] The minimum volume occupied by a dendrimer with N beads with a nonzero excluded volume ν is

$$V_{min} = \nu N = \frac{4}{3}\pi R_{min}^3 \tag{20}$$

where N grows exponentially with increasing generation number. The dendrimer's maximum accessible volume, where it reaches the fully stretched state $R \sim (g+1)s$, grows cubically with the number of generations,

$$V_{max} = \frac{4}{3}\pi(g+1)^3s^3 \tag{21}$$

Since the occupied volume grows faster with g than the accessible volume, it is obvious that there will come a point beyond which the dendrimer cannot grow as a consequence of a lack of space. Hence, our theory is applicable for generations below a certain generation g_{max}. Combining eqs 20 and 21 and solving them numerically, we find an increase in the value of the maximum attainable generation number, $g_{max} = 13$, 16, and 21 for dendrimers with spacer length $s = 1$, 2, and 7, respectively.

Analogous to the definition of a linear chain in a Θ-solvent, where it behaves ideally, a dendrimer θ-point can be defined by taking $\alpha \equiv 1$ and solving eq 16. This gives the dimensionless energy in the θ-point

$$\epsilon_\theta = \frac{1}{\phi_{max} - \phi_0} \tag{22}$$

As already mentioned, the dendrimer can no longer contract to its ideal size if $\phi_0 \rightarrow \phi_{max}$ because $\epsilon_\theta \rightarrow \infty$. The solvent is poor if $\epsilon > \epsilon_\theta$. As follows from eq 22, the

θ-temperature depends on the generation number and spacer length.

Another definition of a θ-point was suggested by Sheng et al.[12] Near the θ-temperature the dendrimer is believed to behave in a quasi-ideal fashion because of an effective cancellation between the attractive and excluded-volume interactions. Nevertheless, the many-body interactions result in more expanded average structure. Since all simulated values of the gyration radius obtained with the help of MC simulations[12] for different temperatures collapse onto a single curve in the good-solvent regime, one can identify the θ-point as the temperature at which data of different generations start to diverge, i.e., as a limiting temperature above which eq 18 still works. Defined in such way the θ-point does not depend on the values of g and s (see section 4.2 for a further discussion).

3.1.2. Dendrimers with Charged Terminal Groups. To calculate the corresponding contribution ΔF_Q to the free energy of a charged dendrimer, we assume that the charged terminal groups are distributed uniformly over the surface of a sphere with radius R. As was shown by MC simulations of Welch and Muthukumar[8] and will be shown by the present BD simulation in section 4.5, the spatial distribution of the charged terminal groups has a very narrow maximum. Therefore, our approximation looks rather reasonable.

The term ΔF_Q may be calculated as the energy of electrostatic interactions between the terminal charge of a single branch and all other charges on the sphere. The expression for ΔF_Q is obtained in Appendix A in the form

$$\frac{\Delta F_Q}{k_b T} = \frac{N_T z^2 \lambda_B k^{-1}}{2R^2}[1 - e^{-2kR}] \tag{23}$$

where N_T is the total number of the charged groups. Thus, the total free energy $F_{F+vdW+Q}$ for a charged dendrimer with excluded-volume interactions may be written as

$$\frac{F_{F+VdW+Q}}{k_b T} = \frac{F_{F+VdW}}{k_b T} + \frac{\Delta F_Q}{k_b T} \tag{24}$$

3.1.3. Non-Gaussian Behavior. For a charged dendrimers each branch may become additionally stretched due to the electrostatic repulsion, to the extent that the Gaussian-spring approximation no longer holds. Therefore, we have to take into account a non-Gaussian overstretching term ΔF_{over} in the free energy instead of pure Gaussian term $^3/_2\alpha^2$ (see Appendix B)

$$\frac{F_{el+over}}{k_b T} = \frac{F_{el}}{k_b T} + \frac{\Delta F_{over}}{k_b T} \tag{25}$$

where

$$\frac{\Delta F_{over}}{k_b T} = -\frac{9}{20}\frac{1}{\sqrt{(g+1)s}}\alpha^3 \ln\left(1 - \frac{\alpha}{\sqrt{(g+1)s}}\right) \tag{26}$$

Note that this is a natural interpolation between the regime of the low stretching ($\alpha \ll 1$) and the overstretched regime ($\alpha \gg 1$). This interpolation slightly underestimates the free energy for $\alpha \to 1$.

The total free energy F of a single linear branch of a charged dendrimer may be rewritten as

$$\frac{F_{tot}}{k_b T} = \frac{F_{el+over}}{k_b T} + \frac{\Delta F_{VdW}}{k_b T} + \frac{\Delta F_Q}{k_b T} \tag{27}$$

Minimization of eq 27 results in the equation for the expansion factor α which are solved numerically both for neutral ($\Delta F_Q = 0$) and charged cases. Both for the neutral and charged dendrimers with spacer length $s = 1, 2, 7$ the numerically obtained maximum generation numbers are close to the maximum generation numbers g_{max} found earlier solving eqs 20 and 21 numerically.

4. Results of Brownian Dynamics Simulation

4.1. Validation of the Mean-Field Approximation. One of the most convenient ways to express the size of a polymer is by means of its mean-squared radius of gyration, $\langle R_g^2 \rangle$. This quantity can be measured, for example, in a small-angle neutron scattering (SANS) experiment[28] and is well-defined for all polymer topologies. For a Gaussian freely jointed dendrimer without excluded-volume interactions the mean-squared radius of gyration, $\langle R_{g0}^2 \rangle$, was derived analytically by La Ferla[29]

$$\langle R_{g0}^2 \rangle = \frac{3[12 \times (2^g) + 4(3g-2)2^{2g} - 1]}{[3(2^{g+1} - 1) + 1]^2} \tag{28}$$

The mean-field approximation used in section 3 is only applicable if the size fluctuations are small. These fluctuations can be quantified by $\Delta_{R_g^2}$

$$\Delta_{R_g^2} = \frac{\mathrm{Var}(R_g^2)}{\langle R_g^2 \rangle^2} = \frac{\langle R_g^4 \rangle - \langle R_g^2 \rangle^2}{\langle R_g^2 \rangle^2} \tag{29}$$

The simulation results for $\Delta_{R_g^2}$ for dendrimers of different generations and different spacer lengths are presented in Figure 3 as a function of decreasing solvent quality. It can be seen that the fluctuations decrease with increasing generation number and are small, especially for large generations, in comparison to the simulated results for the linear Gaussian coil with $N = 129$ beads. Therefore, it can be argued that mean-field approximation, described earlier, is a very reasonable approach, especially for large-generation dendrimers.

4.2. Radius of Gyration of Neutral Dendrimers with Excluded-Volume Interactions. For comparison of the BD results with theoretical predictions one needs to determine the parameters ν and ϵ in eq 15. We relate the parameter ν to the position r_0 of the minimum of the modified Lennard-Jones potential and ϵ to the depth of the potential well

$$\nu = r_0^3 = \left(\frac{2}{\beta_{LJ}}\right)^{1/2}\sigma^3 \tag{30a}$$

$$\epsilon = -U_{LJ}(r_0) = \epsilon_{LJ}\beta_{LJ}^2 \tag{30b}$$

In a good solvent, $\epsilon < \epsilon_\theta$, the excluded-volume interactions cause a dendrimer to swell significantly in comparison to the ideal case (Figure 4a). The dependence of R_g^2 vs N obtained by the BD method for a dendrimer with $s = 2$ is compared with the corresponding MD results of Karatasos et al.[30] They obtained a stronger dependence, which may be related to the higher values of the excluded-volume parameter σ used in their paper.

In Figure 2a,b the expansion factors obtained from the simulation (symbols) and theory (lines) are plotted as functions of the solvent quality for dendrimers with

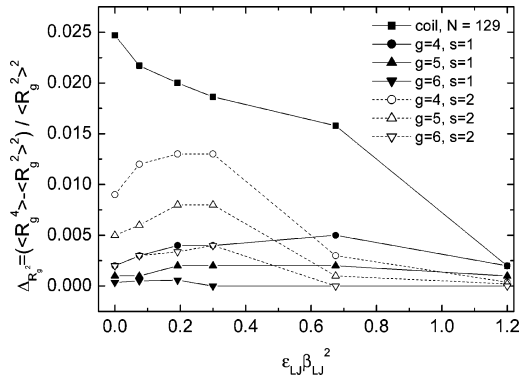

Figure 3. Fluctuations of the mean-squared radius of gyration for neutral dendrimers with different number of generations and different spacer lengths as a function of decreasing solvent quality. BD results for a linear Gaussian chain with $N = 129$ beads are also shown.

spacer lengths $s = 1$ and $s = 2$. Figures 2a,b and 4a show that satisfactory agreement between simulation data and theory predictions is observed for all simulated dendrimers. Only for the athermal solvent (when $\beta_{LJ} = 0$) BD results slightly deviate from the theory.

As shown earlier (see eq 22), the value of $\epsilon = \epsilon_\theta$ cannot be physically reached if $\phi_0 \rightarrow \phi_{max}$. As can be seen from Figure 2a, this is already the case for a $g = 6$ dendrimer with spacer length $s = 1$. As follows from our definition (eqs 13 and 22), ϵ_θ should depend on the generation number and spacer length and therefore on the total number of beads N in the dendrimer. The points where the dependence of the expansion factor α vs ϵ cross the line $\alpha = 1$ differ considerably for different values of g and s. Sheng et al.[12] defined ϵ_θ as an energy at which the scaling relation for good solvents described by eq 18 stops to be valid. The dependence $R_g/(N^{1/5}[s(g+1)]^{2/5}) = \alpha(R_{g0}/N)^{1/5}$ vs ϵ for all considered dendrimers is plotted in Figure 4b. The simulated results do superimpose at ϵ below $\epsilon_\theta \sim 0.3$ and disperse at larger values of ϵ. Therefore, such a definition of the θ-point leads to a value of ϵ_θ which is considerably smaller than the value determined from the relation $\alpha(\epsilon_\theta) = 1$ ($\epsilon_\theta \sim 1$ for $g = 5$, $s = 1$ dendrimer) and is closer to the value of $\epsilon_\theta = 0.3$ for a linear chain.

4.3. Self-Similarity. The structure of dendrimers suggests the possibility of a fractal self-similarity. In the literature the following scaling between the mean-squared radius of gyration and the number of beads has been suggested

$$\langle R_g^2 \rangle \propto N^{2/d_f} \tag{31}$$

where d_f could be considered as fractal dimension. By MD simulation Murat and Grest[6] found the fractal dimension $d_f = 3.3$ for generations $g = 5-8$ dendrimers with spacer length $s = 7$. In an MC simulation of a model lattice dendrimer Mansfield[31] obtained fractal dimensions between 2.45 and 2.76. Figure 4c shows the simulated values of $\langle R_g^2 \rangle$ for $g = 1-5$ neutral dendrimers and the calculated results for $g = 5-8$ dendrimers. It is seen that the slope of curves in Figure 4c is not constant but decreases with the generation number. It means that dendrimers of different generations cannot be considered as objects with the same fractal dimension. Nevertheless, we could describe the simulation dependence of $\langle R_g^2 \rangle$ vs N by eq 31 with a variable effective dimension d_{eff}, which should however not reflect internal scaling. The relation between N and R_g

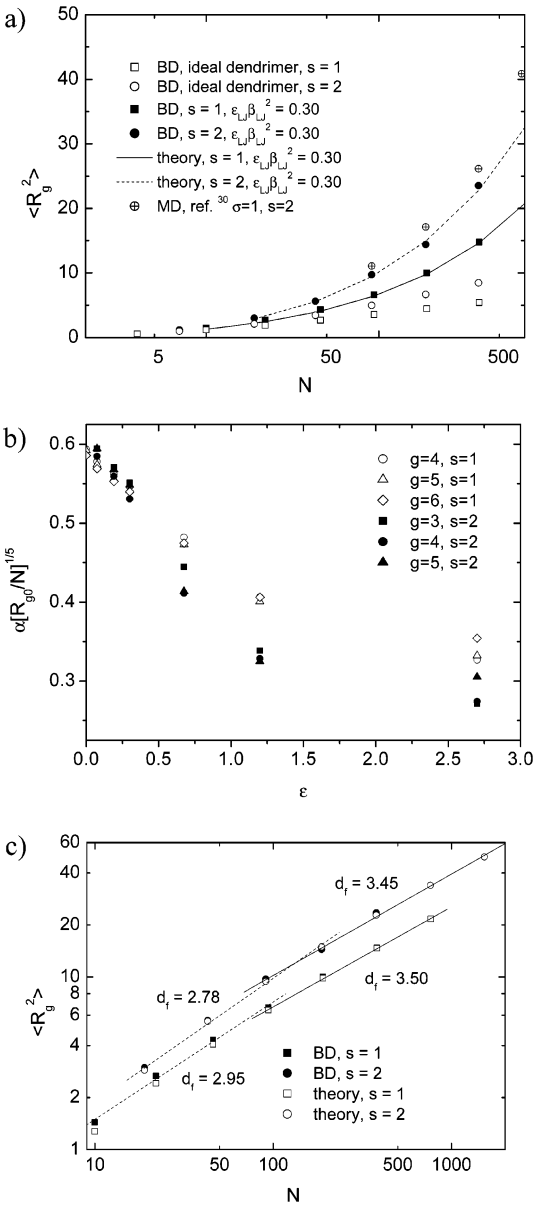

Figure 4. (a) Mean-squared radius of gyration, R_g^2, as a function of number of beads, N, for ideal dendrimers (ID), BD simulation results, and numerical solution of the free energy (eq 27) minimization for neutral dendrimers with spacer lengths $s = 1$ and $s = 2$ in a solvent with $\epsilon_{LJ}\beta_{LJ}^2 = 0.30$. (b) Dependence of $R_g/(N^{1/5}[s(g+1)]^{2/5})$ vs ϵ for all simulated neutral dendrimers. Scaling behavior is clearly seen for $\epsilon < 0.3$. (c) Size exponents for generation $g = 1-8$ dendrimers with spacer lengths $s = 1$ and $s = 2$ in a good solvent, $\epsilon_{LJ}\beta_{LJ}^2 = 0.30$. Dashed lines represent fits to the simulation data, and solid lines represent numerical solution of the free energy (eq 27) minimization.

can be written as $N(R_g) \sim R_g^3\langle\rho(R_g)\rangle$, where $\langle\rho(R_g)\rangle$ is an average monomer density in a dendrimer. For objects with a constant density $d_{eff} = 3$. We obtain that the effective d_{eff} is less than 3 in the region of small generation numbers and increases up to ~3.5 for large generations. Such a behavior shows that the average monomer density decreases with R_g in the region of small N and increases in the region of large N. This densification of dendrimers of high generations is related to the enhanced back-folding of the dendrimer branches due to the excluded-volume interactions.In Figure 5a the mean-field results for the radius of gyration of a dendrimer in a solvent with $\epsilon_{LJ}\beta_{LJ}^2 = 0.30$ are plotted together with the experimental values for a

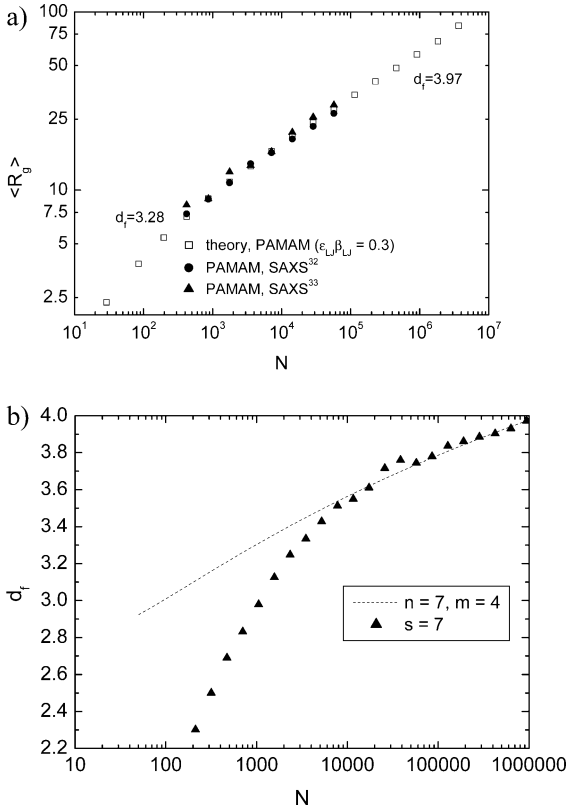

Figure 5. (a) Mean-squared radius of gyration for PAMAM dendrimer of generations $g = 4-g_{max}$; experimental results[32,33] and numerical solution of the free energy (eq 27) minimization. The size exponent d_f is displayed also. (b) Size exponent of a neutral dendrimer with excluded-volume interactions in an overstretched state (dashed line) and numerical solution of the free energy (eq 27) minimization (filled triangles) for a dendrimer with the spacer length $s = 7$.

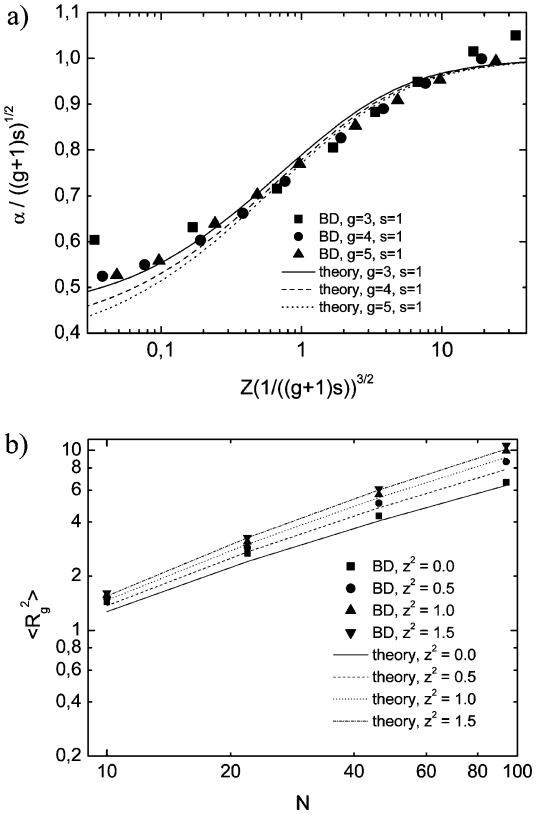

Figure 6. (a) Theoretical (eq 27) and simulation (BD) results for dendrimers $g = 3$, 4, 5 and with spacer length $s = 1$. Excluded-volume interactions are not taken into account. The linear-expansion factor α is scaled with $\sqrt{(g+1)s}$, and the x-axis values are scaled with $(1/3)(z^2\lambda_B N_T/R_{g0})((g+1)s)^{-3/2}$ to obtain a universal curve. (b) Molecular weight dependence of the mean-squared radius of gyration for charged dendrimers in a good solvent, $\epsilon_{LJ}\beta_{LJ}^2 = 0.30$, and for different values of effective charge z.

poly(amidoamine) (PAMAM) dendrimer obtained by SAXS[32,33] and show a very good agreement. For PAMAM the values of the size exponent are 3.28 and 3.97 for generations 4−8 and 8−g_{max}, respectively.

For large generation numbers and $\epsilon < \epsilon_\theta$ the neutral dendrimer is overstretched, and the excluded-volume term in the expression for a free energy is dominant. Taking into account the effective internal density of an ideal dendrimer, $\phi_0 \sim (N/(s \log N)^{3/2})$, and simplifying eq 27, we can rewrite the gyration radius as $R_g^2 \sim N^{2/7}(s \log N)^{8/7} \sim N^{2/d_f}$, where the size exponent d_{eff} can be defined as

$$d_{eff} = \frac{n}{1 + m\,\dfrac{\log(\log N)}{\log N}} \qquad (32)$$

with some integer numbers of m and n ($n = 7$ and $m = 4$ in the high-generation case). The value of the size exponent is plotted in Figure 5b together with the size exponents obtained from the minimization of the free energy (eq 27) for a dendrimer with spacer length $s = 7$. For the high-generation dendrimers the agreement is very good, and we conclude that the dominant contributions to the free energy for a neutral dendrimer are the excluded-volume and overstretching terms.

4.4. Radius of Gyration of Dendrimers with Charged Terminal Groups. To study the influence of the electrostatic interactions on the dendrimer size and structure, we considered two different cases. First, for the case of $\epsilon_{LJ}\beta_{LJ}^2 = 0.3$, we carried out BD simulations with varied effective charge of the terminal groups, ze, keeping the value of Debye length fixed at $k^{-1} = 100$. The variation of the parameter z corresponds to the change of the degree of ionization (or valence) of the terminal groups. In this case the Debye length exceeds the dendrimer size, and almost nonscreened electrostatic interactions are taken into account. Second, for the case of an athermal solvent ($\beta_{LJ} = 0$) the simulations with different Debye length and $z = 1$ have been also performed. Changing the value of Debye length characterizes the change of the electrostatic interactions due to the change of the solvent ionic strength (salt concentration in the solution). As follows from eq 27, for high-g dendrimers the contribution to the free energy from the electrostatic interactions exceeds that from the van der Waals attraction, meaning that at high values of the Debye length the absolute value of the parameter β_{LJ} is not so important.

4.4.1. Simulation Results Obtained by Variation of the Effective Charge of Terminal Groups. The mean-field approximation (see Appendix A) suggests a universal behavior of the scaled linear expansion factor $\alpha/\sqrt{(g+1)s}$ vs $Z((g+1)s)^{-3/2}$, where $Z = (1/3)(z^2\lambda_B N_T/R_{g0})$. To check this scaling behavior, the charged dendrimers without excluded-volume interactions are simulated. Figure 6a indeed shows that the simulation results for $g = 3-5$ dendrimers with spacer length $s = 1$ are in a good agreement with the mean-field theory.

Figure 6b shows the molecular weight dependence of the mean-squared radius of gyration for dendrimers in a solvent with $\epsilon_{LJ}\beta_{LJ}^2 = 0.30$ and for different values of z. The simulation (BD) results are in a good agreement with the mean-field approximation, but the theory slightly underestimates the simulation data.

4.4.2. Simulation Results Obtained by Variation of the Debye Length. BD simulations with different values of the Debye length and fixed Bjerrum length ($\lambda_B = 1$) have been performed for a dendrimer with spacer length $s = 1$ in an athermal solvent ($\beta_{LJ} = 0$). For this case we observe a slight decrease of fractal dimensions for all generations, $d_f = 2.63$ ($k^{-1} = 0.8$) and $d_f = 2.42$ ($k^{-1} = 100$), as compared to the neutral case for the dendrimers of the same generations. It means that charged dendrimer becomes more friable with increase of the range of the electrostatic repulsion, k^{-1}.The simulated dependence of the expansion factor α on the generation number g is shown in Figure 7a both for neutral and charged dendrimers. For the case of almost nonscreened electrostatic interactions ($k^{-1} = 8.96$) the results for the dendrimers of generation $g > 3$ in a solvent with $\epsilon_{LJ}\beta_{LJ}^2 = 0.30$ are very close to those for the athermal solvent. So, the solvent quality is not so important for the swelling of a dendrimer of high generations if electrostatic interactions between all charged groups are taken into account.

The results of the BD simulations at different Debye lengths have been compared with the free energy minimization results, taking into account both the non-Gaussian elongation effect and three- and higher-body excluded-volume interactions. The excluded-volume parameter v of a single bead in eq 27 was determined by eq 30a. However, for neutral dendrimers in athermal solvents (when $\beta_{LJ} \sim 0$) theory deviates from the BD results (see Figure 2). To have better agreement between theory and the results of the computer simulation, the excluded-volume parameter $v = r_{ex}^3$ could be used as a free fitting parameter. For neutral dendrimers the best agreement between the mean-field theory (eq 27) and the simulation results is found for $r_{ex} = 0.56$. Neglecting the non-Gaussian stretching (eq 25) leads to a somewhat smaller value of this fitting parameter, $r_{ex} = 0.46$. The results of the approximation are shown in Figure 7b.

The calculation of the expansion factor for a charged dendrimer is made for a high value of the Debye length, $k^{-1} = 8.96$, comparable to the dendrimer size, where electrostatic interactions are almost nonscreened. In the first approximation we can put radius of the charged sphere equal to the characteristic size of a dendrimer, i.e., to the average radius of gyration of an ideal dendrimer, $R = R_{g0}$. However, as shown in Figure 7c, only theory which takes into account the non-Gaussian stretching gives reasonable agreement with the results of the BD simulation. Gaussian theory gives overestimated values of the expansion factor for all considered dendrimers.

The most probable radius for the localization of the charges in a dendrimer, R_t, can be estimated from the locations of the maxima of the corresponding distribution functions (see section 4.5). For large generations the agreement between BD results and mean-field theory becomes even better if the radius of the charged sphere R is put to be equal to R_t (Figure 7c).

4.5. Density Distribution. De Gennes and Hervet[5] suggested that the monomer radial density is minimal

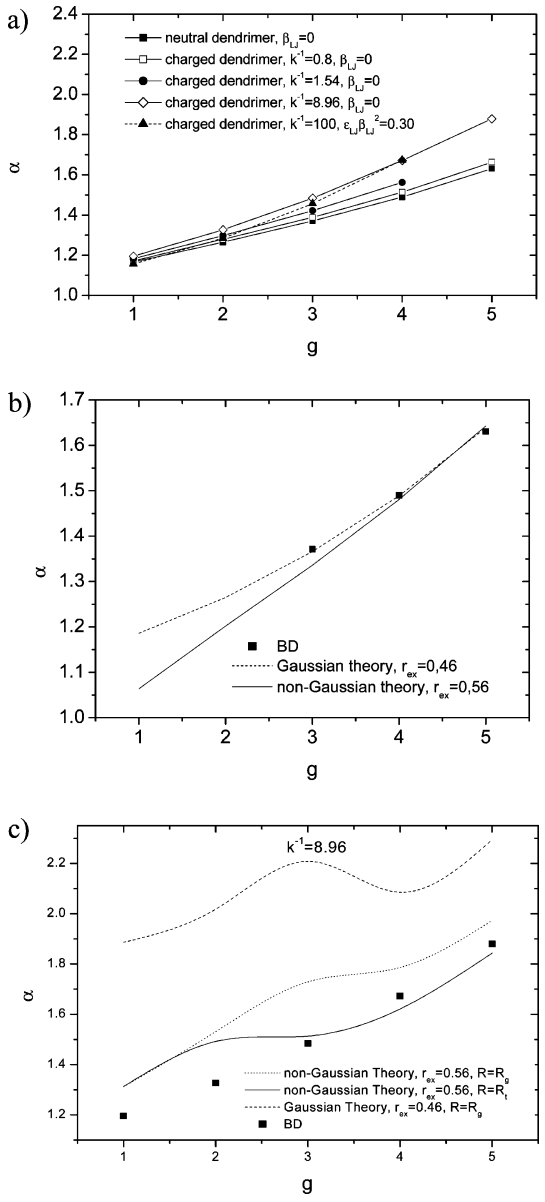

Figure 7. (a) Dependence of the simulated expansion factor $\alpha = R_g/R_{g0}$ on the generation number g for charged dendrimers with different values of the Debye length. (b) Dependence of the expansion factor α on the generation number g for a neutral dendrimer. The values of $r_{ex} = 0.46$ and $r_{ex} = 0.56$ are used as fitting parameters in eqs 24 and 28, respectively. (c) Dependence of the expansion factor α on the generation number g for a charged dendrimer, $k^{-1} = 8.96$. The excluded-volume parameter is taken as $r_{ex} = 0.56$.

at the core and increases monotonically to the periphery of a dendrimer. However, computer simulations[6−8] and theoretical studies[9,10] show that the radial density distribution has a maximum at the core and decreases monotonically with distance. The average number of monomers in each spherical shell at a distance r away from the center, $\rho(r)$, is calculated as

$$\rho(r) = \frac{\langle n(r) \rangle}{V(r)} \tag{33}$$

where $\langle n(r) \rangle$ is the average number of beads at a distance r and $V(r)$ is the volume of the shell.

4.5.1. Radial Monomer Distribution Function for Neutral Dendrimers. In Figure 9 the radial monomer distribution functions of dendrimers with $g = 5$ and s

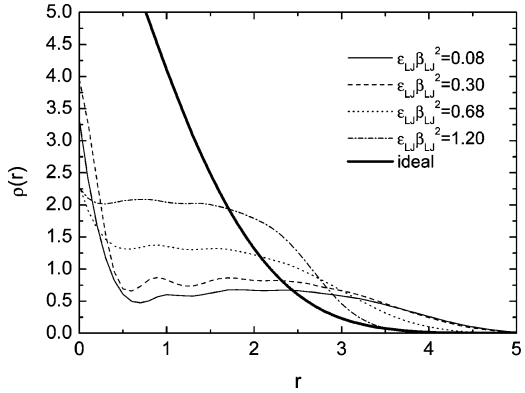

Figure 8. Radial monomer distribution function as a function of solvent quality for neutral dendrimers with $g = 5$, $s = 1$. Qualitatively the same picture is valid for the case $s = 2$.

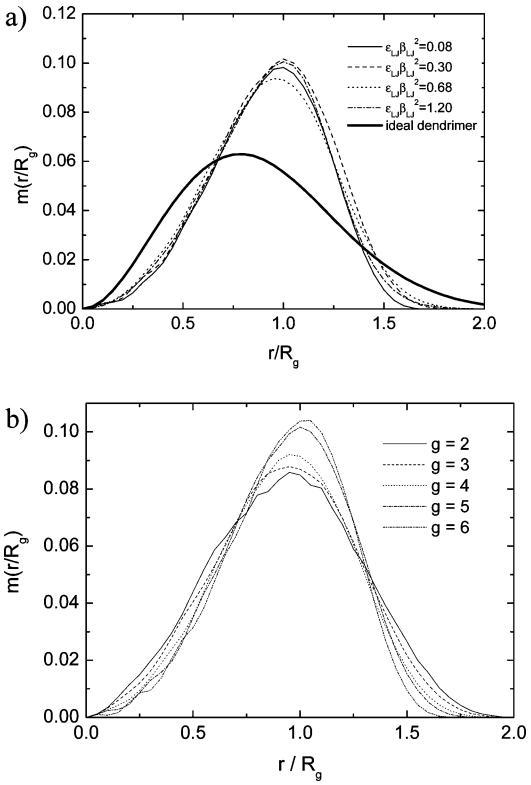

Figure 9. (a) Radial mass distribution as a function of solvent quality for a neutral dendrimer with $g = 5$, $s = 1$. The radial mass distribution of an ideal dendrimer is plotted as a reference. (b) Radial mass distribution function of neutral dendrimers with spacer lengths $s = 1$ and generation $g = 2-6$ in a solvent with $\epsilon_{LJ}\beta_{LJ}^2 = 0.30$. Qualitatively the same pictures are valid for the case $s = 2$.

$= 1$ are shown for different solvent qualities. The simulations show a significant difference in the microscopic structure of ideal and nonideal dendrimers. Both ideal and nonideal dendrimers show a maximum in the core region. However, where the ideal dendrimer shows a monotonic decrease toward the periphery, the density distribution of the nonideal dendrimer decreases quickly to a local minimum, whereafter there is a plateau toward the edge and then a monotonic decrease again. Qualitatively, this picture remains the same for $s = 2$ and for solvents of different quality. In the last case only the widths and the absolute values of the plateaus differ.

4.5.2. Radial Mass Distribution for a Neutral Dendrimer. From the definition of the radial monomer distribution function $\rho(r)$ we have

$$N = \int \rho(r) 4\pi r^2 \mathrm{d}r = R_g{}^3 \int \rho(r/R_g) 4\pi (r^2/R_g{}^2)\, \mathrm{d}(r/R_g) \tag{34}$$

where the distance r is normalized by the dendrimer's radius of gyration R_g. The radial mass distribution can be defined as

$$m(r/R_g) = (R_g{}^3/N)\rho(r/R_g)(r^2/R_g{}^2) \tag{35a}$$

In Figure 9a the radial mass distributions of neutral dendrimers with $g = 5$, $s = 1$ are shown for different solvent qualities. The radial mass distributions of the dendrimers show a universal scaling behavior for different solvent qualities and different spacer lengths. The mass distribution function is Gaussian, with its maximum located at $r/R_g \sim 1$, and differs from the distribution function of an ideal dendrimer. The distribution function remains Gaussian even for dendrimers of lower generations (Figure 9b). Qualitatively, the same pictures are valid for the case $s = 2$.

Murat and Grest[6] suggested to estimate a fractal dimension of a dendrimer from the following scaling relation

$$M(r/R_g) = M(r') \sim r'^{d_f} \tag{35b}$$

where the integral radial mass distribution function $M(r') = \int_0^{r'} 4\pi\tilde{r}^2\rho(\tilde{r})\, d\tilde{r}$ is the number of beads which are located within a sphere of radius r'. The dependence of M on r/R_g is shown in Figure 10 for dendrimers with different number of generations and $s = 1$. It is seen that the power law, eq 35b, is valid for the internal structure of a single dendrimer at $r/R_g < 1$, but the value of d_f increases with increasing generation number, from $d_f \sim 2.5$ ($g = 2$) to $d_f \sim 3.1$ ($g = 6$). Qualitatively, the same behavior is observed for the dendrimers with $s = 2$ for which the value of the exponent d_f lies between 2.5 and 2.8.

4.5.3. Localization of Terminal Groups. The localization of the terminal groups is important because many practical applications of dendrimers rely on the availability of these groups. Many computational and theoretical studies predict backfolded structures of separate dendrons. Recently, a SANS contrast-variation experiment of a poly(propyleneamine) $g = 4$ dendrimer with deuterated terminal groups was carried out by Rosenfeldt et al.[34] They convincingly demonstrated that an appreciable number of terminal groups are folded back into the interior of the molecule. Present BD simulations also show that the terminal beads are evenly dispersed throughout the whole dendrimer (Figure 11).

4.5.4. Radial Monomer Distribution Function for a Charged Dendrimer. The neutral dendrimer is dense at the inside while the charged dendrimer is much more open. This can be seen from the radial density distribution function for dendrimers with different effective charge of the terminal groups and Debye length, as shown in Figures 12a and 13a. At small radial distances local minima arise, while at the same time an increase of the effective charge z or Debye length shifts the distribution of the terminal groups to the right (Figures 12b and 13b); this could be expected, as charge−charge repulsions are minimized by forcing the charged monomers as far apart as possible.

4.6. Static Structure Factor. The scattered radiation intensity as studied by a small-angle neutron

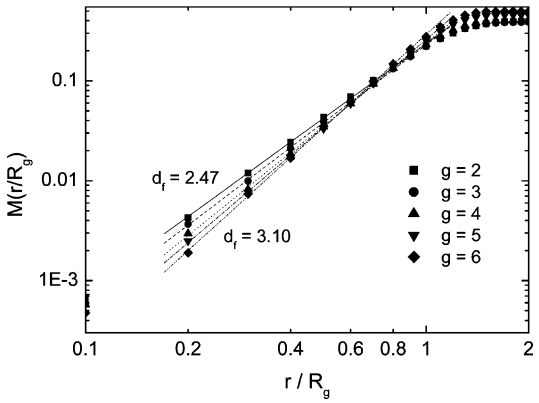

Figure 10. Integral radial mass distributions $M(r/R_g)$ of neutral dendrimers with spacer lengths $s = 1$ and generation $g = 2-6$ in a solvent with quality $\epsilon_{LJ}\beta_{LJ}^2 = 0.30$. Lines represent fits to the simulation data, eq 35b. Qualitatively the same picture is valid for the case $s = 2$.

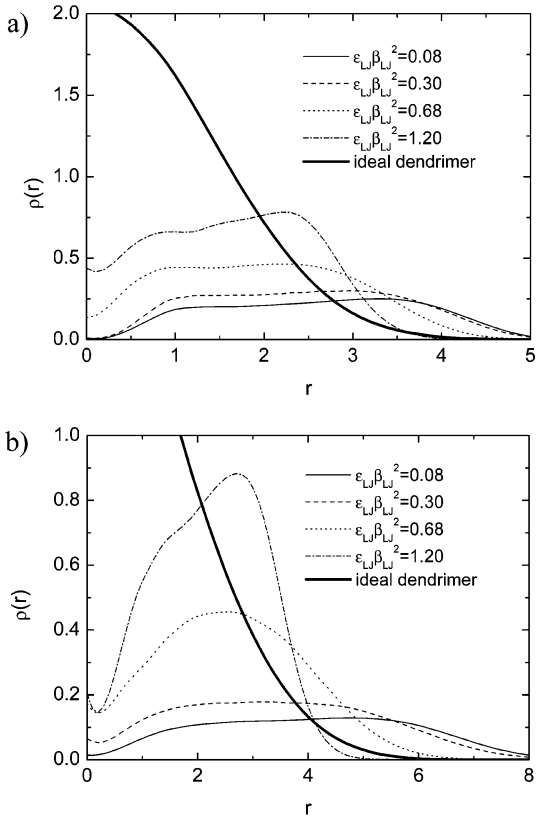

Figure 11. Radial distribution function of terminal groups as a function of solvent quality for neutral dendrimers with $g = 5$, $s = 1$ (a) and $g = 5$, $s = 2$ (b).

scattering (SANS) experiment is proportional to the static structure factor

$$S(q) = \langle |\sum_{n=1}^{N}\sum_{m=1}^{N} e^{i\vec{q}\cdot(\vec{r}_n - \vec{r}_m)}|^2 \rangle \qquad (36)$$

which is measured directly in the present simulations. Here $\vec{q}$ is the scattered radiation vector, $q = |\vec{q}| = (4\pi/\lambda)\sin(\Omega/2)$, Ω is the scattering angle, λ is the wavelength, and $\vec{r}_n$ are the coordinates of the scattering centers.In Figure 14a, the structure factor $S(q)$ for $g = 1-6$ dendrimers with spacer length $s = 1$ is displayed in a Kratky plot representation and compared with the theoretical predictions for a Gaussian coil and a sphere.

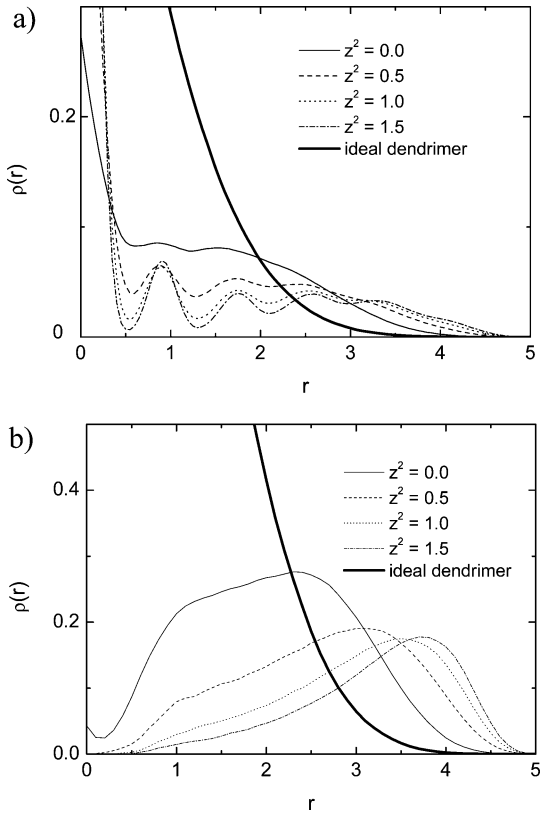

Figure 12. Radial monomer density distribution (a) and distribution of terminal groups (b) for a dendrimer with $g = 4$ and $s = 1$ at different values of the effective charge z. $k^{-1} = 0.01$, $\epsilon_{LJ}\beta_{LJ}^2 = 0.30$.

With increasing generation number the structure factor curves show more and more similarity with an ideal sphere. Obtained results are in a good agreement with MD simulations of Karatasos et al.[30] and with MC simulation of Giupponi and Buzza.[35] For a dendrimer with $s = 1$, Karatasos et al.[30] found the major peak in a Kratky presentation at $qR_g = 1.7$, close to the value of qR_g in the present simulations. The secondary peak is resolved here at $qR_g = 4.8$, which is the same as that obtained by Karatasos[30] and Giupponi and Buzza.[35] In SANS experiments of Scherrenberg et al.[28] and of Ramzi et al.[36] the secondary peak is also observed in the range of $qR_g \cong 4-5$.

In Figure 14b, the Kratky plot representation is shown for charged dendrimers with $g = 4$ and $s = 1$ and with different effective charge z. With increasing z the curve oscillates more and shifts upward. This suggests that dendrimers become more spherical but also less dense at the inside, which agrees with the changes seen in the radial distribution. Qualitatively, the same picture is valid for the case $s = 2$.

4.7. Shape of a Dendrimer. Denoting the coordinates of the mth bead by $x_k^{(m)}$, $k = 1, 2, 3$, the symmetrical shape tensor, **Q**, can be defined as[37]

$$Q_{kl} \equiv \frac{1}{N}\sum_{m=1}^{N} x_k^{(m)} x_l^{(m)} - \frac{1}{N^2}\sum_{m=1}^{N} x_k^{(m)} \sum_{n=1}^{N} x_l^{(n)} \qquad (37)$$

The trace of **Q** equals the squared radius of gyration and the spread in **Q**'s eigenvalues $\lambda_1 \geq \lambda_2 \geq \lambda_3 \geq 0$ measures the polymer's asymmetry. Aronovitz and Nelson[38] derived two extra parameters to characterize

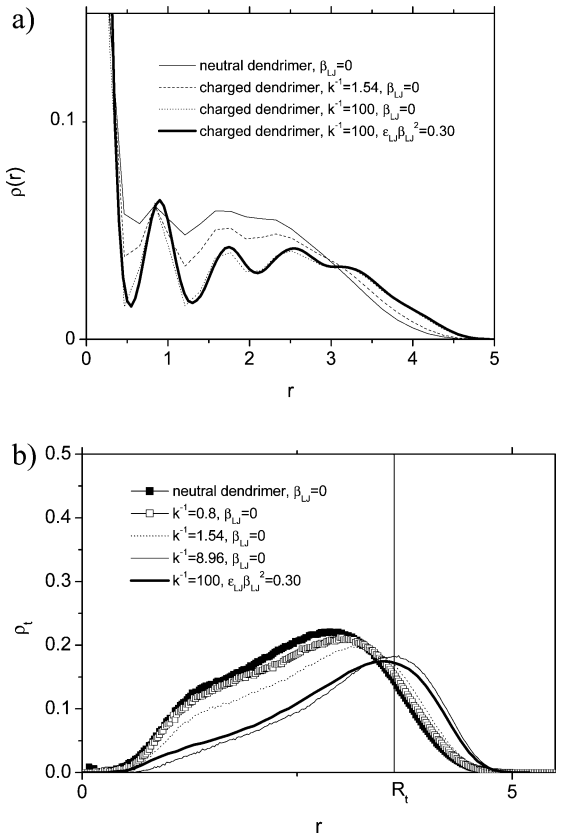

Figure 13. Radial monomer density distribution (a) and distribution of terminal groups (b) for a dendrimer with $g = 4$ and $s = 1$ at different values of the Debye length ($\lambda_B = 1$) in an athermal solvent, $\beta_{LJ} = 0$. The results for $\epsilon_{LJ}\beta_{LJ}^2 = 0.30$ and for a high value of the Debye length are presented for comparison.

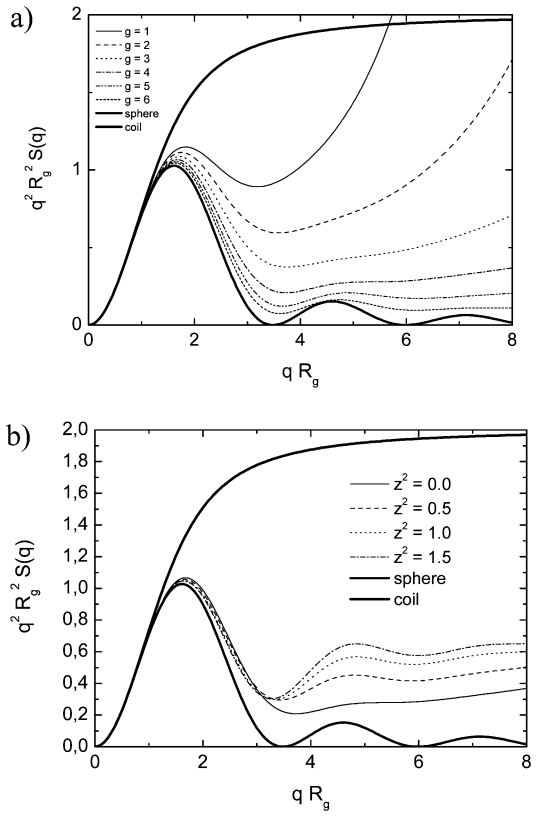

Figure 14. (a) Kratky plot representation of the structure factor $S(q)$ for neutral dendrimers with $g = 1-6$ and $s = 1$, $\epsilon_{LJ}\beta_{LJ}^2 = 0.30$. (b) Kratky plot representation for charged dendrimers with $g = 4$ and $s = 1$ for different values of z. $k^{-1} = 0.01$. Qualitatively the same pictures are valid for the case $s = 2$.

the polymer's shape. An additional traceless matrix $\hat{\mathbf{Q}}$ is defined by

$$\hat{\mathbf{Q}} = \mathbf{Q} - \bar{\lambda}\mathbf{I} \tag{38}$$

with

$$\bar{\lambda} = \text{tr } \mathbf{Q}/3 \tag{39}$$

Using this matrix, a degree of asymmetry is defined as

$$\Delta = \frac{2}{3}\frac{\langle \text{tr } \hat{\mathbf{Q}}^2 \rangle}{\langle (\text{tr } \mathbf{Q})^2 \rangle} \tag{40}$$

where $0 \le \Delta \le 1$; $\Delta = 0$ for spherical and $\Delta = 1$ for linear objects. The prolateness/oblateness is defined by

$$S = 27\frac{\langle \det \hat{\mathbf{Q}} \rangle}{\langle (\text{tr } \mathbf{Q})^3 \rangle} \tag{41}$$

where $-1/4 \le S \le 2$; $S = 0$ for spherical objects. In Figure 15, the asymmetry factor Δ (a) and prolateness/oblateness factor S (b) for neutral dendrimers with spacer lengths $s = 1$ and $s = 2$ are plotted. It can be seen that the asymmetry rapidly disappears for high-generation dendrimers, so they can be considered as dense spherical objects.

5. Conclusions

For high-generation dendrimers, $g \ge 3$, the BD simulations show that the dendrimers hardly fluctuate. Therefore, we assume that a mean-field theory will be a good approximation. In addition to previous theoretical efforts of Boris and Rubinstein[9] and of Ganazzoli et al.,[10] we included three-body and higher-order excluded-volume interactions into the mean-field approximation to predict the conformational properties of the dendrimers near the starburst limit and in particular the swelling and collapse with varying solvent quality. The mean-field approximation shows very good agreement with the results of the BD simulations for the swelling and collapse of neutral dendrimers well below the starburst limit. On the basis of this, a definition of the dendrimer θ-point is derived from the theory, which shows that a dendrimer can no longer contract to its ideal size for high generation numbers.

The Gaussian approximation fails for charged dendrimers in athermal solvents because the branches in the dendrimer are strongly stretched. Therefore, an additional elastic free energy term which corrects for the overstretching is included. Experimental data of the PAMAM dendrimer could be fitted very well using the numerical solutions of this total free energy expression.

For the approximation of the additional Coulomb free energy term, we assumed a smooth distribution of charged terminal groups on a spherical object. From the results of the BD simulation of dendrimers with electrostatic interactions but without excluded-volume interactions, we can conclude that this approximation is very reasonable. From the numerical solutions of the full free energy expression of charged dendrimers, we see that there is no significant influence of the charges on the radius of gyration of the dendrimer.

The present computer simulations have been performed at constant Bjerrum length. At constant tem-

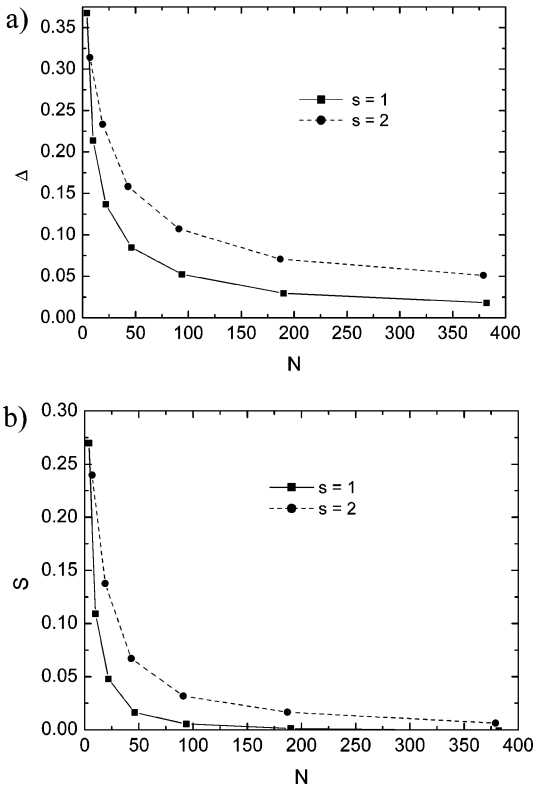

Figure 15. Asymmetry factor Δ (a) and prolateness/oblateness factor S (b) as functions of number of beads for neutral dendrimers with spacer lengths $s = 1$ and $s = 2$, $\epsilon_{LJ}\beta_{LJ}^2 = 0.30$.

perature this corresponds to a fixed value of the dielectric constant for dendrimers with different number of generations. The effective dielectric constant inside a dendrimer can depend on the monomer density, which changes with g. This effect needs a special study and could be a subject of a future investigation; first, indications from the present work are that the effect will be not that significant, since we observe a rather weak R dependence of the average dendrimer density. For high-g dendrimers the possible counterions condensation in the salt-free (unscreened limit) regime could decrease the effective charge density. However, a high degree of ionization of terminal groups was observed also[15] for a dilute water solution of poly(amidoamine) dendrimers with small salt concentration (in this case the screening length exceeded the dendrimer size). We can add to this some recent experience from Monte Carlo simulation of a model dendrimer with explicit counterions.[42] It was shown that in the unscreened regime the counterion condensation starts when the ratio of the Bjerrum length to the spacer length is larger than unity. In the present study this ratio is equal to unity. Therefore, we do not expect a noticeable counterion condensation.

Comparing the results of the present BD simulations with MC simulations of Lue[39] and MD simulations of Murat and Grest,[6] we observe a good qualitative agreement. The radial density distribution functions of neutral dendrimers have maximum at the core, then a monotonic decrease with some plateau toward the edge, and then a monotonic decrease again. The influence of charges on the radial distribution is significant. Additional minima and maxima appear with increase of the effective charge z or/and Debye length, which correspond to an increase of the internal stress of the dendrimer. The dendrimer core is then hollow, and the terminal groups are shifted to the periphery.

We studied the fractal properties of neutral dendrimers in two different ways: by determining (i) the exponent in the scaling law $R_g^2 \propto N^{2/d_f}$ for dendrimers of different generations and (ii) the exponent in the scaling law $M(r) \propto r^{d_f}$ for a given generation number. The dendrimers of different generations cannot be considered as fractal objects with the same fractal dimensions.

In the Kratky plot representation of the structure factor it can be easily seen that high-generation dendrimer shows much similarity with an ideal spherical object. Two parameters to characterize a polymer's shape are derived from the gyration tensor—the asymmetry and prolateness/oblateness. For high-generation dendrimers the dendrimer becomes very symmetric and almost spherical. The sphericity of the dendrimer increases also by charging its terminal groups.

Acknowledgment. Grateful acknowledgment is made to Dr. K. Zeldovich (Moscow State University) and to Dr. I. Neelov and Prof. T. Birshtein (Institute of Macromolecular Compounds, St. Petersburg) for many useful discussions. This work was carried out with the financial support of the NWO Grant 047.009.017, ESF program SIMU, RFBR Grants 02-03-33135 and 03-03-06379, and INTAS Grant 00-712.

Appendix A. Charged Dendrimers

A.1. Derivation of the Free Energy of Charged Terminal Groups. In the first approximation we suppose that the dendrimer with ionized terminal groups may be represented as a charged spherical surface with radius R. The energy of the electrostatic interactions of one single charge with all other charges can be written in the Debye approximation as

$$\frac{\Delta F_Q}{k_b T} = \int \rho \frac{z^2 \lambda_B}{r} e^{-kr} dS \qquad (A.1)$$

Here dS is the surface element, ρ is the surface charge density, z is the numerical charge of one bead, r is the distance between charges, $r = 2R \sin(\theta/2)$, R is the radius of the sphere, and θ is the usual polar angle in spherical coordinates. By assumption of the uniform distribution of N_T charges over the sphere, the surface density $\rho$is equal to

$$\rho = \frac{N_T}{4\pi R^2} \qquad (A.2)$$

After simple calculations the additional term in the free energy corresponding to the electrostatic interactions is written as

$$\frac{\Delta F_Q}{k_b T} = \frac{N_T z^2 \lambda_B k^{-1}}{2R^2}[1 - e^{-2kR}] \qquad (A.3)$$

A.2. Charged Dendrimers without Excluded-Volume Interactions. Equation 27 may be simplified if electrostatic and elastic terms are dominant and the excluded-volume term can be neglected. For weakly screened electrostatic interactions (high values of the Debye length k^{-1}) eq A.3 is simplified to

$$\frac{\Delta F_Q}{k_B T} = 3Z\frac{1}{\alpha} \tag{A.4}$$

where $Z = (1/3)(z^2\lambda_B N_T/R_{g0})$. Away from the overstretched limit the total free energy of a single linear branch becomes

$$\frac{F}{k_b T} = \frac{F_{el}}{k_b T} + \frac{\Delta F_{conf}}{k_b T} + \frac{\Delta F_Q}{k_b T} \tag{A.5}$$

The linear expansion factor α could be obtained by minimizing the free energy:

$$\alpha - \alpha^{-1} - Z\alpha^{-2} = 0 \tag{A.6}$$

From the solution of eq A.6 we can distinguish three regimes: (1) weakly stretched regime, where $\alpha = 1 + \delta$

$$\delta = \frac{1}{6}\frac{\lambda_B N_T}{R_{g0}} \le 1 \tag{A.7}$$

(2) strongly stretched regime, where the first term (stretching) and third term (Coulomb interactions) in eq A.6 are dominant

$$\alpha = Z^{1/3} \gg 1 \tag{A.8}$$

(3) overstretched regime, where the first and second term in (A.6) are dominant

$$\alpha \ge (g+1)^{1/2} \tag{A.9}$$

In that case, $R_g > (g+1)s$, and this is not physically possible. Therefore, we correct for the overstretching in the same way as in the starburst limit and include an additional term for the elastic free energy. The total free energy of a single linear branch in an end-charged dendrimer is given by

$$\frac{F_{no-VdW}}{k_b T} = \frac{F_{el}}{k_b T} + \frac{\Delta F_{conf}}{k_b T} + \frac{\Delta F_{over}}{k_b T} + \frac{\Delta F_Q}{k_b T} \tag{A.10}$$

The condition for the linear expansion factor α reads

$$\left(\frac{\alpha}{\sqrt{(g+1)s}}\right)^3 - \frac{9}{20}\left(\frac{\alpha}{\sqrt{(g+1)s}}\right)^4 \ln\left(1 - \frac{\alpha}{\sqrt{(g+1)s}}\right) + \frac{3}{20}\left(\frac{\alpha}{\sqrt{(g+1)s}}\right)^5 \frac{1}{1 - \frac{\alpha}{\sqrt{(g+1)s}}} - gs\frac{\alpha}{\sqrt{(g+1)s}} = Z((g+1)s)^{-3/2} \tag{A.11}$$

For $Z((g+1)s)^{-3/2} \le 1$ the same solutions must be found as without the additional elastic term in the free energy. Then we have for $(\alpha/\sqrt{(g+1)s} \ll 1$

$$\left(\frac{\alpha}{\sqrt{(g+1)s}}\right)^3 - \left(\frac{\alpha}{\sqrt{(g+1)s}}\right)((g+1)s)^{-1} = Z(g+1)^{-3/2} \tag{A.12}$$

with the expected solutions: (i) weakly stretched regime, $Z \le 1{:}\alpha \cong 1 + (1/2)Z$, and (ii) strongly stretched regime, $Z \ge 1{:}\alpha \cong Z^{1/3}$. For $Z(g+1)^{-3/2} \ge 1$ and $\alpha/\sqrt{(g+1)s} \to 1$ we find the overstretched regime and

$$\alpha \cong \sqrt{(g+1)s}\left(1 - \frac{1}{Z(g+1)^{-3/2}}\right) \tag{A.13}$$

Appendix B. Strongly Stretched Freely Jointed Linear Chain. The partition function of a stretched linear chain, with $N = (g+1)s$ beads connected by rods of length b can be written as[40]

$$\frac{Q(R,N,b)}{Q(0,N,b)} = \left[\frac{\sinh L^{-1}\left(\frac{R}{Nb}\right)}{L^{-1}\left(\frac{R}{Nb}\right)}\right]^N \exp\left[-\frac{R}{b}L^{-1}\left(\frac{R}{Nb}\right)\right] \tag{B.1}$$

where $L(x) \equiv \coth x - (1/x) \sim 1 - (1/x)$. In the case of a strongly stretched chain the partition function can be further simplified, and if $R \sim Nb$, the contribution to the free energy is given by (ignoring terms not depending on R):

$$-\frac{\Delta F_{str}}{k_b T} \cong -N\ln\left(1 - \frac{R}{Nb}\right) \tag{B.2}$$

So long as the polymer is not near its starburst limit, $(R/Nb) \ll 1$, the chain behaves Gaussian. The free energy can then be written as[41]

$$\frac{\Delta F_G}{k_b T} = \frac{3}{2}\left(\frac{R}{\sqrt{N}b}\right)^2 + \frac{9}{20}N\left(\frac{R}{Nb}\right)^4 \tag{B.3}$$

A natural interpolation between the Gaussian limit and the strongly stretched regime is given by

$$\frac{F_{el+over}}{k_b T} = \frac{F_{el}}{k_b T} - \frac{9}{20}N\left(\frac{R}{Nb}\right)^3 \ln\left(1 - \frac{R}{Nb}\right) \tag{B.4}$$

Substitution of $N = (g+1)s$ and $b = 1$ gives the final expression for the elastic free energy:

$$\frac{F_{el+over}}{k_b T} = \frac{F_{el}}{k_b T} + \frac{\Delta F_{over}}{k_b T} = \frac{3}{2}\alpha^2 - \frac{9}{20}\frac{1}{\sqrt{(g+1)s}}\alpha^3 \ln\left(1 - \frac{\alpha}{\sqrt{(g+1)s}}\right) \tag{B.5}$$

References and Notes

(1) Buhleier, E. W.; Wehner, W.; Vogtle, F. *Synthesis* **1978**, *1978* (2), 155.
(2) Tomalia, D. A.; Baker, H.; Dewald, J. R.; Hall, M.; Kallos, G.; Martin, S.; Roeck, J.; Ryder, J.; Smith, P. *Polym. J.* **1985**, *17*, 117.
(3) Tomalia, D. A.; Baker, H.; Dewald, J. R.; Hall, M.; Kallos, G.; Martin, S.; Roeck, J.; Ryder, J.; Smith, P. *Macromolecules* **1986**, *19*, 2466.
(4) Liu, M. J.; Frechet, M. J. *Pharm. Sci. Technol. Today* **1999**, *2*, 393.
(5) De Gennes, P. G.; Hervet, H. *J. Phys., Lett.* **1983**, *44*, 351.
(6) Murat, M.; Grest, G. *Macromolecules* **1996**, *29*, 1278.
(7) Welch, P.; Muthukumar, M. *Macromolecules* **1998**, *31*, 5892.
(8) Welch, P.; Muthukumar, M. *Macromolecules* **2000**, *33*, 6159.
(9) Boris, D.; Rubinstein, M. *Macromolecules* **1996**, *29*, 7251.
(10) Ganazzoli, F.; La Ferla, R.; Terragni, G. *Macromolecules* **2000**, *33*, 6611.
(11) Flory, P. J. *Principles of Polymer Chemistry*, Cornell University Press: Ithaca, NY, 1953.
(12) Sheng, Y.-J.; Jiang, S.; Tsao, H.-K. *Macromolecules* **2002**, *35*, 7865.
(13) Kabanov, V. A.; Zezin, A. B.; Rogacheva, V. B.; Gulyaeva, Zh. G.; Zansochova, M. F.; Joosten, J. G. H.; Brackman, J. *Macromolecules* **1999**, *32*, 1904.

(14) Kabanov, V. A.; Sergeyev, V. G.; Pyshkina, O. A.; Zinchenko, A. A.; Zezin, A. B.; Joosten, J. G. H.; Brackman, J.; Yoshikawa, K. *Macromolecules* **2000**, *33*, 9587.
(15) Nisato, G.; Ivkov, R.; Amis, E. J. *Macromolecules* **2000**, *33*, 4172.
(16) Lyulin, A. V.; Davies, G. R.; Adolf, D. B. *Macromolecules* **2000**, *33*, 3294.
(17) Lyulin, A. V.; Davies, G. R.; Adolf, D. B. *Macromolecules* **2000**, *33*, 6899.
(18) Lyulin, A. V.; Adolf, D. B.; Davies, G. R. *Macromolecules* **2001**, *34*, 3783.
(19) Lyulin, A. V.; Adolf, D. B.; Davies, G. R. *Macromolecules* **2001**, *34*, 8818.
(20) de la Torre, J. G.; Rey A.; Freire, J. J. *Macromolecules* **1987**, *20*, 342.
(21) Lee, I.; Athey, B. D.; Wetzel, A. W.; Meixner, W.; Baker, J. R. J. *Macromolecules* **2002**, *35*, 4510. Nisato, G.; Ivkov, R.; Amis, E. J. *Macromolecules* **1999**, *32*, 5895. van Duijvenbode, R. C.; Borkovec, M.; Koper, G. J. M. *Polymer* **1998**, *39*, 2657.
(22) Allen, M. P.; Tildesley, D. J. *Computer Simulations of Liquids*; Clarendon Press: Oxford, 1987.
(23) Ermak, D. L.; McCammon, J. A. *J. Chem. Phys.* **1978**, *69*, 1352.
(24) Ryckaert, J.-P.; Bellemans, A. *Chem. Phys. Lett.* **1975**, *30*, 123.
(25) Ryckaert, J.-P.; Ciccotti, G.; Berendsen, H. J. C. *J. Comput. Phys.* **1977**, *23*, 327.
(26) Grosberg, A. Yu.; Khokhlov, A. R. *Statistical Physics of Macromolecules*, AIP Press: New York, 1994.
(27) Birshtein, T. M.; Pryamitsyn, V. A. *Macromolecules* **1991**, *24*, 1554.
(28) Scherrenberg, R.; Coussens, B.; van Vliet, P.; Edouard, G.; Brackman, J.; de Brabander, E. *Macromolecules* **1998**, *31*, 456.
(29) La Ferla, R. *J. Chem. Phys.* **1997**, *106*, 688.
(30) Karatasos, K.; Adolf, D. B.; Davies, G. R. *J. Chem. Phys.* **2001**, *115*, 5310.
(31) Mansfield, M. L. *Polymer* **1994**, *35*, 1827.
(32) Prosa, Ty. J.; Bauer, B. J.; Amis, E. J.; Tomalia, D. A.; Scherrenberg, R. *J. Polym. Sci.* **1997**, *35*, 2913.
(33) Prosa, Ty. J.; Bauer, B. J.; Amis, E. J. *Macromolecules* **2001**, *34*, 4897.
(34) Rosenfeldt, S.; Dingenouts, N.; Ballauff, M.; Werner, N.; Vogtle, F.; Lindner, P. *Macromolecules* **2002**, *35*, 8098.
(35) Giupponi, G.; Buzza, D. M. A. *Macromolecules* **2002**, *35*, 9799.
(36) Ramzi, A.; Bauer, B.; Scherrenberg, R.; Froehling, P.; Joosten, J.; Amis, E. *Macromolecules* **1999**, *32*, 4983.
(37) Solc, K. *J. Chem. Phys.* **1971**, *55*, 335.
(38) Aronovitz, J. A.; Nelson, D. R. *J. Phys. (Paris)* **1986**, *47*, 1445.
(39) Lue, L. *Macromolecules* **2000**, *33*, 2266.
(40) Hill, T. L. *An Introduction to Statistical Thermodynamics*; Dover: New York, 1986.
(41) Volkenshtein, M. V. *Configurational Statistics of Polymer Chains*; Interscience Publishers: New York, 1963.
(42) Galperin, D.; Mazo, M.; Ivanov, V.; Khokhlov, A. *Preprints of Papers*; 3rd International Kargin Conference, Moscow, Moscow State University, Jan 27−Feb 1, 2004; p 212.

MA035286H